Computers and Electronics in Agriculture 226 (2024) 109420

Contents lists available at ScienceDirect

Computers and Electronics in Agriculture

journal homepage: www.elsevier.com/locate/compag

Original papers

Three-dimensional image analysis for almond endocarp feature extraction and shape description

Marco Sánchez-Beeckman [a,1,*], Jaume Fornés Comas [b,1], Onofre Martorell [a], José M. Alonso Segura [c], Antoni Buades [a]

[a] Institute of Applied Computing and Community Code (IAC3) and Department of Mathematics and Computer Science, Universitat de les Illes Balears, Cra. de Valldemossa km. 7.5, Palma, 07122, Spain
[b] Departament de Biologia, Universitat de les Illes Balears, Cra. de Valldemossa km. 7.5, Palma, 07122, Spain
[c] Estación de Examen DHE. Centro de Investigación y Tecnología Agroalimentaria de Aragón (CITA), Av. Montañana 930, Zaragoza, 50059, Spain

ARTICLE INFO

Keywords:
Almond endocarp
3D imaging
Feature extraction
Surface description
Geometric measure

ABSTRACT

We propose a morphological characterization of the endocarp of the fruit of the almond tree, *Prunus amygdalus* (Batsch), using computer vision techniques to extract features in 3D almond endocarp meshes with the objective to describe the diversity of the crop in a systematic and unambiguous form. All the proposed descriptors are quantitative and easily computable, allowing fast and objective assessments of the morphological variations between almond varieties. We collect and 3D-scan a total of 9510 almond endocarps to obtain such meshes, to which we apply an affine transformation so that they are positioned in a standardized reference where meaningful physical measures can be taken. Complex descriptors derived from the geometry of the endocarp are then introduced to identify richer features. The use of 3D, compared to simply taking 2D images, allows for a more accurate and complete description of the endocarp shape. In particular, the contour and apex shapes, keel development, markings on the surface, and symmetry of the endocarp are analyzed and given quantitative measures. The validity of the presented morphological descriptors is finally tested on 2610 endocarps from the collected dataset, corresponding to 36 autochthonous almond varieties from the island of Mallorca (Spain) and 14 international reference varieties, all with well documented characteristics. Numerical results show that the proposed descriptors agree with human-made shape classifications of the studied varieties with a coincidence of 75.0 % for contour shape, 76.0 % for apex shape, and 80.0 % for keel development. Visual comparisons of the extracted features also show that they are coherent with commonly used guidelines for the morphological characterization of the almond endocarp. We conclude that the use of 3D imaging approaches for the description of the almond endocarp is a promising alternative to traditional methods, providing a reliable way to deal with ambiguity and helping reduce biases and inconsistencies caused by subjective visual evaluations.

1. Introduction

The almond tree, *Prunus amygdalus* (Batsch), is a widespread crop in areas with a Mediterranean climate, and one of the most important tree-nuts worldwide in terms of commercial production (Food and Agriculture Organization of the United Nations, 2023). Over 1.67 million tons of almond kernels were produced worldwide in 2022 (International Nut & Dried Fruit, 2023), with production concentrating mainly in the USA, Australia, Spain, Turkey, Tunisia, Portugal, Morocco, Chile, and Italy. Being a healthy and functional food (Barreca et al., 2020), the consumption of almond nuts is increasing year by year, especially in countries like India, China, UAE, Japan, and South Korea. This has lead to an increase in their production.

However, in some places with a long history and tradition on their growth, such as the island of Mallorca (Spain), almond cultivation is at a serious risk as a result of the bacterial disease caused by *Xylella fastidiosa* (Moralejo et al., 2020), which is compromising the traditional landscape of the island's countryside and the high diversity of the almond germplasm (Esterlich, 1907; Sacarès i Mulet, 1992). A correct varietal description is essential for the preservation of these genetic resources to ensure crop production and to meet growing environmental

* Corresponding author.
E-mail addresses: marco.sanchez@uib.cat (M. Sánchez-Beeckman), jaume.fornes@uib.cat (J. Fornés Comas), o.martorell@uib.cat (O. Martorell), jmalonsos@aragon.es (J.M. Alonso Segura), toni.buades@uib.cat (A. Buades).
[1] Co-first authors.

https://doi.org/10.1016/j.compag.2024.109420
Received 11 July 2023; Received in revised form 15 February 2024; Accepted 29 August 2024
Available online 4 September 2024

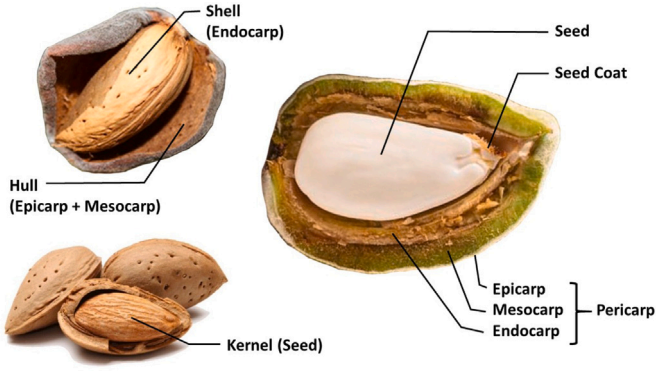

Fig. 1. Parts of the fruit of the almond tree.

challenges and climate change (Socias i Company and Felipe, 1992; Socias i Company et al., 2012).

Most well-known varieties of almonds have a varietal description made by governmental plant variety offices to distinguish between them. However, access to this information is usually not public, and most local varieties have not yet been adequately described (Fornés Comas et al., 2019).

The guidelines of the International Union for the Protection of New Varieties of Plants (UPOV) are the current standard for the description of the morphological traits of the almond tree (UPOV, 2019). The International Board for Plant Genetic Resources (IBPGR) also provides a set of descriptors to characterize it (IBPGR, 1985). In fruit species, the description of fruit traits is a very relevant part of the varietal description. The fruit of the almond (Fig. 1) is a drupe, of which the only edible part is the kernel (or seed), composed by an embryo (two cotyledons) surrounded by a skin (or testa). The pericarp, which encloses the kernel, contains a green, fleshy hull (epicarp and mesocarp) and a hard, pitted shell—the endocarp (Gradziel, 2010). The genetic diversity of the almond germplasm is clearly manifested in the morphological variability of the endocarps, with the description of the characteristics of the endocarps being very valuable information for varietal distinction.

Traditional methods for the morphological description of the almond endocarp are based on its observation and subsequent comparison with the traits of a set of reference varieties. A scale and a digital meter are used for quantitative measurements, while pseudo-qualitative traits are described based on a subjective visual assessment. In particular, morphological traits of interest for the endocarp include the shape of its contour, the shape of its apex, the development of its keel, and the appearance of its markings. These characteristics and all their defined pseudo-qualitative states of expression are shown respectively in Figs. 2, 3, 4, and 5. Yet, such methodology has certain limitations. For instance, in the case of the latter traits, each individual state of expression needs to be identified to adequately describe the range of the characteristic (UPOV, 2002). Different evaluators, depending on their experience and judgment, can give distinct interpretations of the same characteristic, which might lead to inconsistencies in its description. Morphological variation due to the influence of environmental conditions can further complicate varietal description (Grasselly and Crossa-Raynaud, 1980), especially when the differences between states of expression are subtle.

There are many works on the study of almond germplasm from different locations that are based on the UPOV and IBPGR descriptors. Examples can be found in Iran (Ardjmand et al., 2014; Sepahvand et al., 2015), Sardinia (Lovicu et al., 2001), Tunisia (Gouta et al., 2009), Morocco (El Hamzaoui et al., 2014), Lebanon (Chalak et al., 2007) and the Apulia region in Italy (de Giorgio et al., 2007). More complex measurements of traits such as mass, volume, diameter, projected area

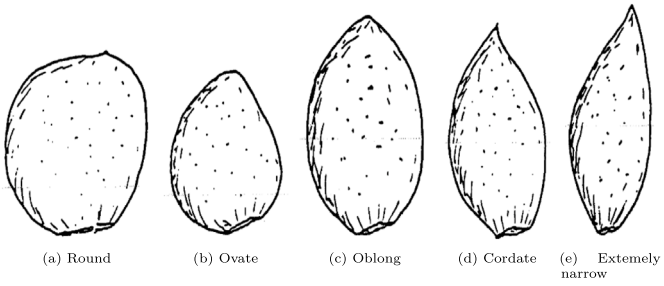

Fig. 2. Reference description for the contour shape of the almond endocarp. *Source:* IBPGR (1985)

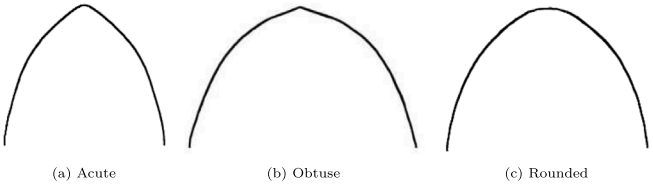

Fig. 3. Reference description for the apex shape of the almond endocarp. *Source:* UPOV (2019)

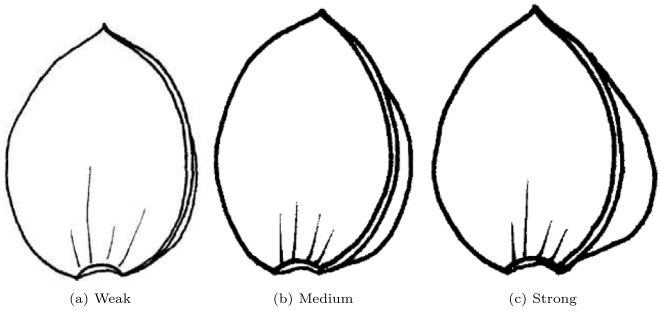

Fig. 4. Reference description for the development of the keel. *Source:* UPOV (2019)

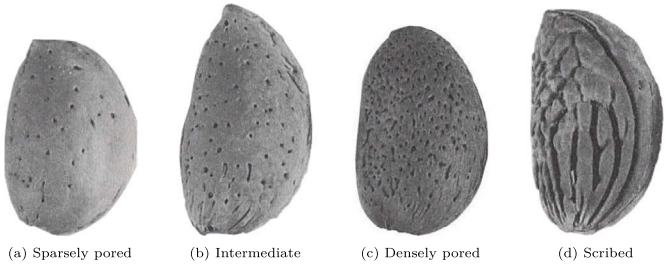

Fig. 5. Reference description for the markings of the almond endocarp. *Source:* IBPGR (1985)

and various proportions have been used to study Iranian (Mohamadi et al., 2010), Moroccan (Sakar et al., 2019) and Portuguese (Oliveira et al., 2018) crops, with the aim of minimizing the subjective bias that exists if only visual comparisons with reference figures are carried out. Taking a step further, a study in Serbia has used image editing tools to extract leaf area (Colic et al., 2012).

The use of imaging techniques for the study of fruit tree crops is becoming more and more widespread. Some studies on almond endocarps use Elliptic Fourier Analysis to define and discriminate between shape groups according to their contour (Antonucci et al., 2012; Demir et al., 2019). Likewise, in the agri-food industry, Zhang and Wu (2012) propose an approach for food classification using supervised

learning methods in digital images. Other works, like those of Halac et al. (2017) and Benarous (2020), also refer to the classification of almond endocarps by characteristics such as quality, size, or state of preservation.

Many other products are being studied with advanced computer vision techniques aswell, from fruits to nuts to cereals (Costa et al., 2011). Similar imaging strategies as those used on almonds have been used with the walnut (Ercisli et al., 2012), the olive (Blazakis et al., 2017; Ponce et al., 2018), and the plum—where Sarigu et al. (2017) explore up to 134 morpho-colorimetric and textural features. Newer works on olive variety recognition (Miho et al., 2024) signal the trend toward the use of deep learning-based imaging methods in the study of plant varieties.

There also exist software tools to perform analysis on various fruits. Tomato Analyzer (Rodríguez et al., 2010) has been developed to extract the namesake fruit's features and facilitate its characterization. SHAPE (Iwata and Ukai, 2002) and GrainScan (Whan et al., 2014) are able to attribute quantitative descriptors to the shape of various seeds and fruits. However, some limitations arise when trying to describe more complex geometrical features like surface roughness and curvature.

In recent years, three-dimensional images have started to become the basis for some applications in agriculture used to describe fruits and seeds (Vázquez-Arellano et al., 2016). Although older related works can be found on the study of soybean (Sakai and Yonekawa, 1992), *Citrus* (Ding et al., 2000), and to assess anthracnose lesions on mango (Corkidi et al., 2006), technological advances in both hardware and software have permitted a more rapid progression on the field of study in the last few years. Particularly, numerical models on 3D images were recently used to extract geometric information of cucumber fruits (Anders et al., 2019), and to characterize phenotypic parameters on strawberries (He et al., 2017). The latter fruit's shape uniformity was also subsequently studied in a later work (Li et al., 2020).

The state of the art is currently moving toward integrating classical imaging approaches with those in three dimensions. A combined strategy using both 2D and 3D images was used in Kyoto University's Experimental Farm (Kusumi et al., 2021) for the study of persimmon. The SHAPE software was used on the bidimensional data to describe the fruit's shape, while 3D models were used to measure complex geometric structures. The same authors continue their research using three dimensional analysis to study developmental mechanisms underlying the complex shape diversity of the fruit (Kusumi et al., 2023). In other recent works, Manolikaki et al. (2022) have compared and complemented 2D and 3D-based methods to characterize 50 scanned olive varieties, based on 8 traits of the fruit and its endocarp. On almonds, however, comparable techniques have yet to be used.

The proposed work follows the aforementioned trend and focuses on the morphological characterization of the almond endocarp using computer vision techniques on 3D meshes. The main objective is to provide continuous quantitative measures for its description, richer than the standard qualitative ones given by the UPOV and the IBGPR so as to reflect the diversity of the crop, yet still easily interpretable and comparable, to characterize it in a systematic and unambiguous form. To accomplish it, we make use of scanned 3D models of almond endocarps and develop new algorithms to extract different features of the geometry of their surface, which we convert into meaningful numerical data. While throughout the work we mainly employ self-obtained scans of a set of almond varieties mostly originating from Mallorca—an island with an important almond genetic diversity pool (Morey and Fornés Comas, 2021)—to test the capabilities of the methods, the techniques are universal and so can be applied to any almond endocarp scan. As far as we are aware, this is the first work on the computational characterization of almonds that uses their geometric properties in 3D space, thus making the research completely novel.

2. Materials

2.1. Almond endocarps

Samples of almond nuts were collected by identifying—with the help of farmers and farm owners—trees known to correspond to different varieties in multiple municipalities of Mallorca. The harvest was done on the maturity period of the nut, when the external hull can be easily separated from the endocarp. For each of the selected trees, around 200 almond nuts were harvested, of which 10 were chosen to be subsequently scanned. The selected nuts were stored in cold conditions (+4 °C) and low relative humidity, in order to preserve them correctly before scanning. Apart from the collected almond nuts, we also included samples of imported almond varieties provided from various research institutions. In total, 9510 almond nuts were selected for scanning.

2.2. 3D scanning

Each nut was scanned individually using a Shining EinScan-SP 3D desktop scanner[2] immediately after measuring its endocarp's width, thickness and length with a digital caliper Z503576-1EA with an accuracy of mm0.1 (Sigma-Aldrich). The scanner is composed of a fixed light source and a turntable, and it uses phase shift structured light to capture the geometry of a static object. The turntable is used to rotate the object, while the light source—a Digital Light Processing (DLP) projector—captures the object from different angles with a single shot accuracy of less than 0.05 mm. The software provided by the manufacturer (EXScan S) is used to control the scanner and to automatically merge the captured images into a 3D mesh of the object.

The obtained 3D endocarp meshes were saved in STL format, discarding color information, for their usage as inputs for the algorithms presented in Section 3. Then, out of all the 9510 meshes, a total of 2610 scans distributed among 50 selected varieties (36 autochthonous from Mallorca and 14 international reference varieties) were chosen to be used as validation data to assess the adequacy of the algorithms for feature extraction. Fig. 6 shows an example of a 3D mesh of each of these varieties viewed from two different angles, alongside a ruler for scale. These 50 varieties were selected so as to coincide with those present in the databases from either the Institut de Recerca i Formació Agroalimentària i Pesquera de les Illes Balears (IRFAP[3])–an administrative organization affiliated to the Conselleria d'Agricultura, Pesca i Medi Natural of the Government of the Balearic Islands–, or the Centro de Investigación *y* Tecnología Agroalimentaria del Gobierno de Aragón (CITA[4])—the accredited center by the Community Plant Varieties Office (CPVO) to carry out Distinctness, Uniformity and Stability (DUS) tests of new almond varieties. Both of these institutions characterize these varieties according to the UPOV Almond DUS guidelines (UPOV, 2019) and the IBPGR almond descriptors (IBPGR, 1985).

3. Method

3.1. Scanning and preprocessing of the 3D meshes

The process of scanning each of the selected almond endocarp is performed in two steps. First, the endocarp is placed on the turntable of the scanner, lying on its side with its keel to the right (like the left examples in Fig. 6 if seen from above). In this position, 8 captures are taken at 45 degree intervals while the turntable rotates automatically in the horizontal axis. Then, the endocarp is manually rotated 90 degrees vertically to lie on its back, with the keel facing upward (right examples

[2] https://www.einscan.com/einscan-sp/
[3] https://varietatslocalsib.com/ca/
[4] https://www.cita-aragon.es/

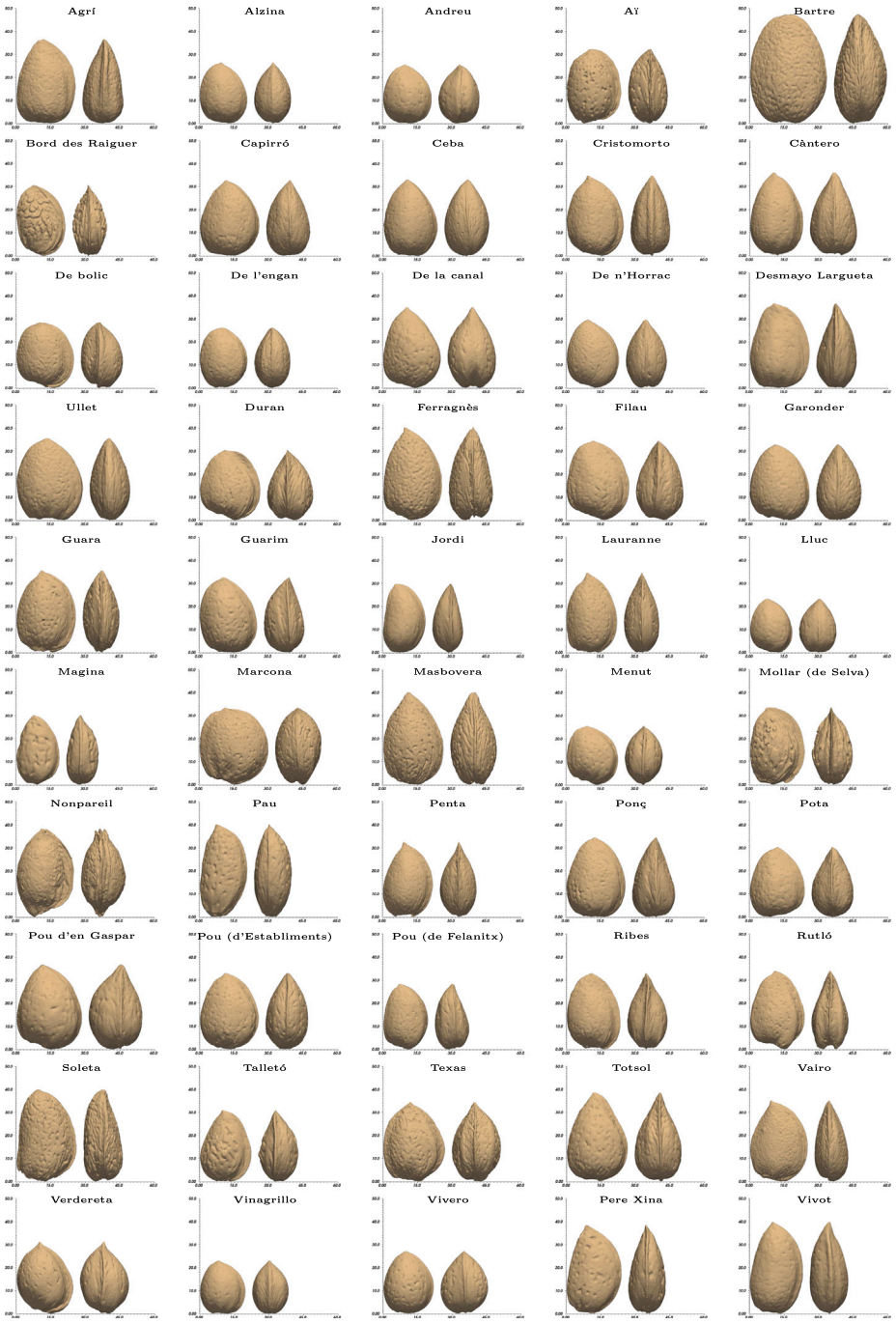

Fig. 6. Example of an almond endocarp of each collected variety, with its name on top. For each endocarp, we show its lateral (left) and front (right) views alongside a ruler to measure its dimensions. Units are in millimeters.

in Fig. 6). Another 8 captures are taken in this position. The resulting 16 captures are then aligned and merged into a single 3D mesh using the software provided with the scanner.

To guarantee that the computation of the descriptors is performed on a common frame of reference, we position each mesh so that the center of the peduncle (the base of the endocarp) is located on the origin of coordinates $O = (0, 0, 0)$, and the apex (its highest point) lies on the positive side of the y-axis. We develop a Python program based on the PyVista library to do so (Sullivan and Kaszynski, 2019).

Given a mesh of an almond endocarp in an arbitrary position and orientation, we manually mark three unaligned key points that should lie on the same plane: the peduncle P, the apex A, and any third point B on the ventral suture. This spanning plane splits the almond endocarp in two almost-equal parts by the ventral suture (as seen in the second row of Fig. 7), and thus can be used as a baseline to orient it with an appropriate isometric transformation. If $\mathbf{u}$ and $\mathbf{v}$ are the unit vectors facing respectively A and B from P, $\mathbf{n} = \frac{\mathbf{u}\times\mathbf{v}}{|\mathbf{u}\times\mathbf{v}|}$ is the unit normal vector to the aforementioned plane, and $\mathbf{w} = \mathbf{n}\times\mathbf{u}$, then the mapping

$$X \mapsto O + \mathbf{M}^T(X - P), \quad \text{where } \mathbf{M} = \begin{bmatrix} n_1 & u_1 & w_1 \\ n_2 & u_2 & w_2 \\ n_3 & u_3 & w_3 \end{bmatrix} \tag{1}$$

positions the mesh the desired way.

Placing the almond endocarp as described, we define its views as the 2D images resulting from the projection of the 3D mesh into the different coordinate planes, as seen in Fig. 7. The front and back views

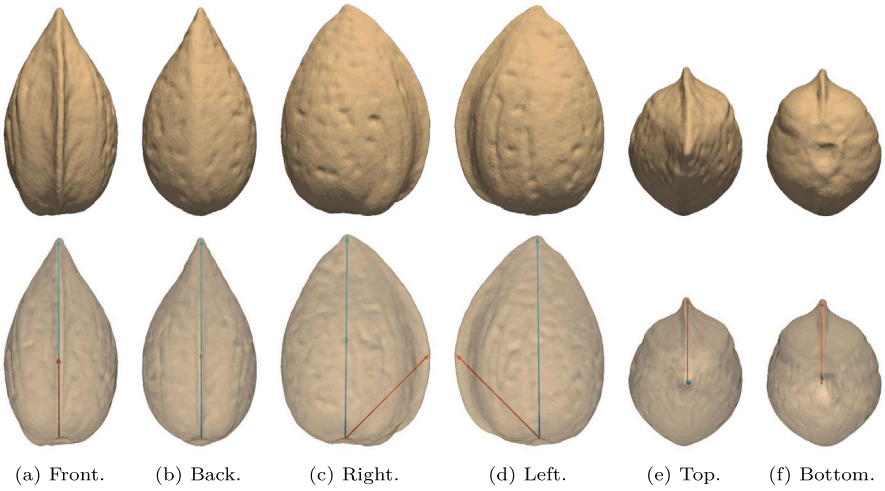

Fig. 7. 3D views of an almond endocarp mesh of the Rutló variety. The bottom row shows the vectors used to position the mesh. These vectors go from the peduncle to the apex (blue arrow) and from the peduncle to the ventral suture (red arrow).

are defined as looking at the mesh perpendicular to the plane xy from different directions; the right and left lateral views, perpendicular to the plane zy; and the top and bottom views, perpendicular to the plane xz.

On the oriented mesh, we can define some relevant points of the endocarp. We consider the top and bottom points, P_t and P_b, as the points with largest and smallest y coordinate, respectively. The left and right points in the front view, P_l^f and P_r^f, are defined similarly using their x coordinate. Likewise, the left and right points in the lateral view, P_l^l and P_r^l, are the points with largest and smallest z coordinate.

3.2. Physical measures

The basic physical measures of interest of the almond endocarp are its length, width, thickness, area and volume. Since we have previously oriented the meshes, it is straightforward to compute all of these traits. Thus, we define:

- The length L as the absolute difference between coordinate y of points P_t and P_b. This can be interpreted as the height of the box of minimal area with sides parallel to the coordinate axes that completely contains the almond endocarp.
- The width W as the absolute difference between coordinate x of points P_l^l and P_r^l.
- The thickness T as the absolute difference between coordinate z of points P_l^f and P_r^f.
- The area and volume of the almond endocarp as those of the closed surface defined by the mesh, which can be computed as in Zhang and Chen (2001).

While these measures are not used directly in this work to describe the almond endocarp, we use them in the definition of some of the proposed continuous quantitative descriptors that follow.

3.3. Feature extraction and description

Among the geometric features of the almond endocarp, we study its contour shape and that of its apex, the development of its keel, the markings on its surface, and its symmetry viewed from different perspectives. In this section, we propose computational methods to obtain meaningful quantitative descriptors to facilitate the characterization of these features. We implement these algorithms in Python using the PyVista framework. Note that to study the keel and the markings, we make use of the full 3D mesh of the almond endocarp, while for the other traits, we project it to its different 2D views. Although the algorithms for the latter could be adapted to work on sets of photographs, projecting the 3D mesh is more precise, guarantees that the endocarps are aligned and at the same scale, and avoids problems derived from perspective and illumination changes.

Contour shape. According to the Almond Test Guidelines (UPOV, 2019), the shape of the lateral view of the almond endocarp (characteristic 34) can be ovate, elliptic, circular or obovate. This classification has shown to be too narrow, as it does not reflect the great diversity of shapes that exist in the wild. The IBPGR (1985) specifies a more realistic classification, dividing almond endocarps into five categories (characteristic 6.2.13): round, ovate, oblong, cordate, and extremely narrow (see Fig. 2). Even though this division is more accurate, it can still be difficult to distinguish between some of these categories when examining some varieties visually. We propose to use instead a combination of two quantitative measures—eccentricity and ovacity—to describe the trait numerically.

The process to obtain these measures is summarized in Fig. 8. We first remove the mucron of the endocarp from all computations. Since all the almond endocarps are centered and oriented such that the vector from the peduncle to the apex is completely straight, we can study the elongation of the endocarp by considering the vertical ellipse inscribed in its lateral view's bounding box. That way, given $a = \max(L, W)$ and $b = \min(L, W)$, we define the eccentricity of the endocarp as that of the aforementioned ellipse,

$$e = \sqrt{1 - \frac{b^2}{a^2}}, \tag{2}$$

so that high (resp. low) values of e correspond to elliptical or narrow (resp. circular or ovate) shapes. We also describe how the width of the endocarp is distributed along its vertical axis with its ovacity

$$\mathcal{O} = \frac{|Q_y - P_y|}{L}, \tag{3}$$

where P_y and Q_y are the vertical components of the center of mass of the endocarp and the center of the ellipse, respectively. That way, endocarps with an evenly distributed width (usually round or oblong ones) have an ovacity value close to 0. The opposite happens to ovate or cordate ones, whose lower center of mass increases the value in (3).

Apex shape. The apex is the highest region of the almond endocarp. The UPOV (2019) establishes three categories to describe its shape on the lateral view of the endocarp, defined in characteristic 35: rounded, acute, and obtuse (see Fig. 3). Visually, the latter two have a distinct sharp point where lines meet at an angle, while the former lacks such a pointed feature and instead presents a smoother shape, similar to the rest of the contour. We precisely quantify this by measuring the roundness of the apex and the angle of its tip, as in Fig. 9.

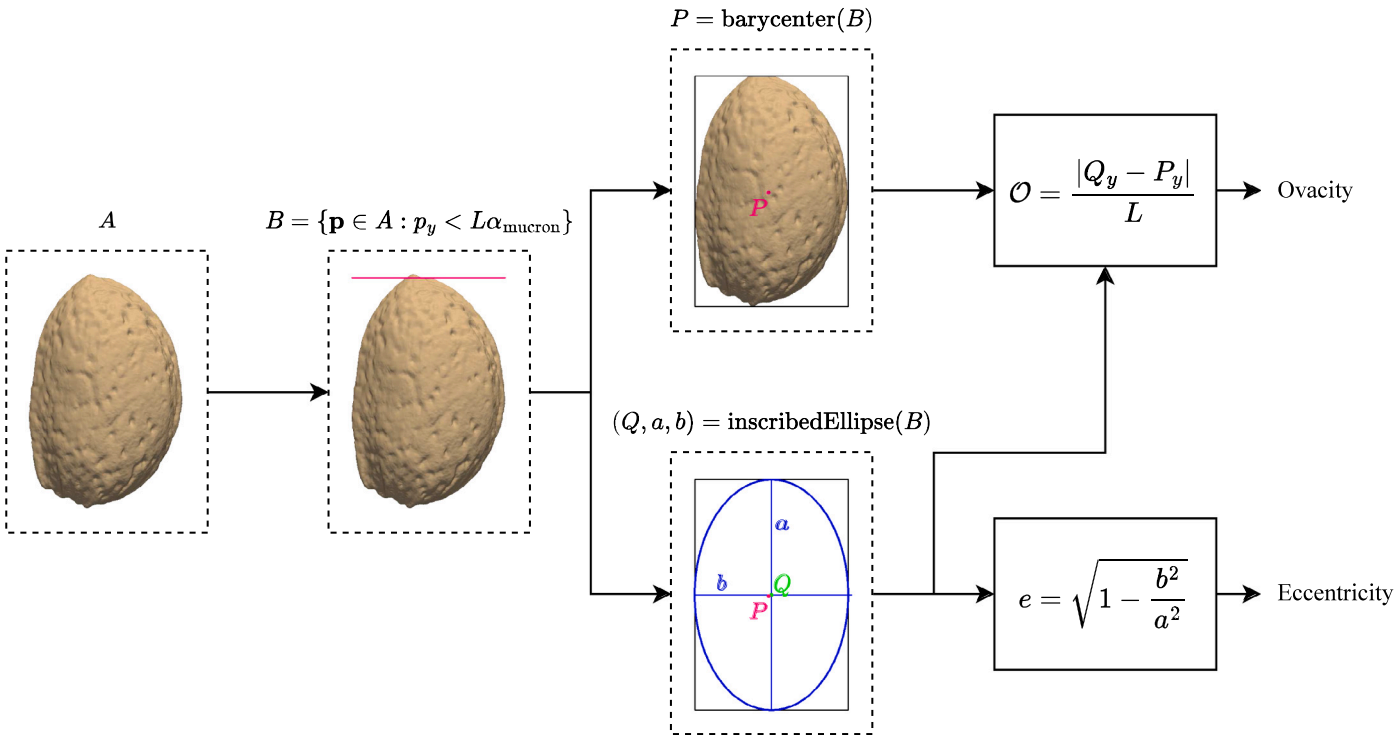

Fig. 8. Process for the description of the contour shape of the almond endocarp. Notation: p_y indicates the component y of point $\mathbf{p}$; α_{mucron} is a parameter pointing to the position of the mucron relative to the length L of the endocarp.

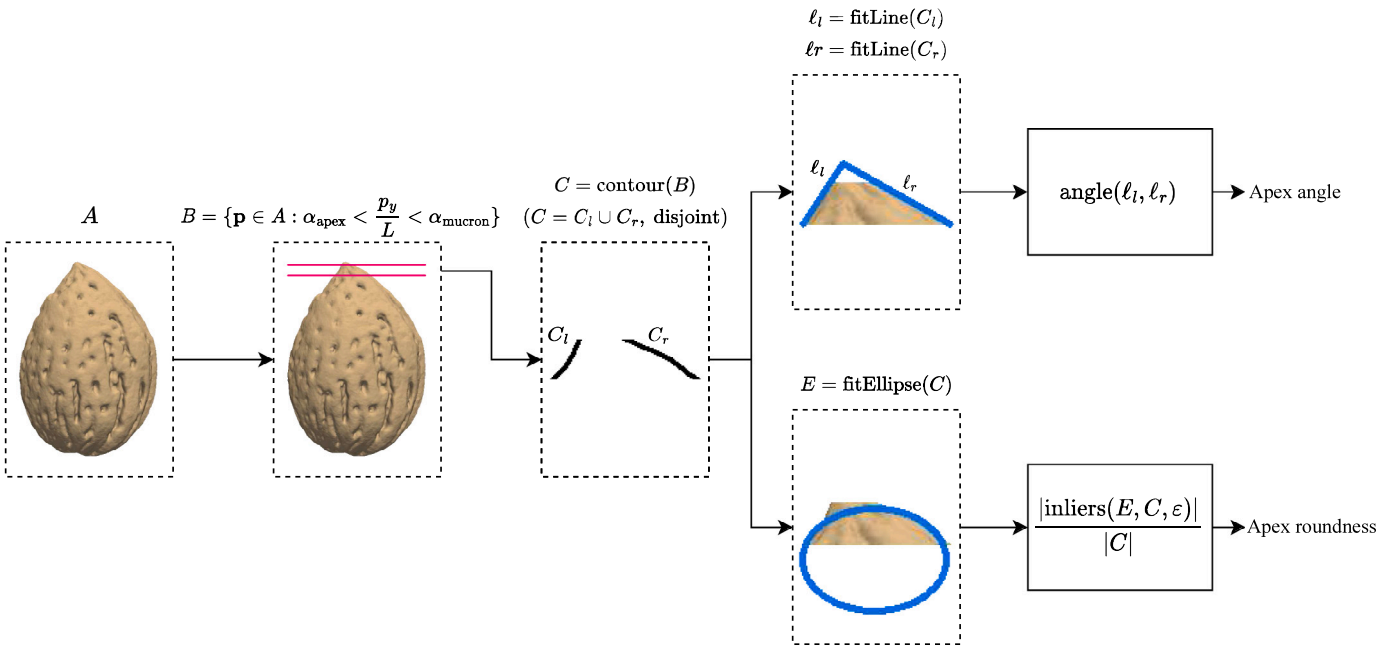

Fig. 9. Process for the description of the apex of the almond endocarp. Notation: p_y indicates the component y of point $\mathbf{p}$; α_{apex} and α_{mucron} are parameters locating the apex and the mucron relative to the length L of the endocarp; ε is a threshold used to determine whether points of the ellipse are close enough to the apex to be considered inliers.

Given the lateral view of the endocarp, we remove the mucron and extract the contour of the topmost region. This leaves two disconnected sets of points, for each of which we fit a line using a classical least squares method. We define the angle of the apex as the inner angle between these two lines. Simultaneously, we fit a non-rotated ellipse (i.e. with null quadratic xy term) using a RANSAC strategy as described in Halíř and Flusser (1998) and Fischler and Bolles (1981). We define the apex roundness as the proportion of inliers in the ellipse model over the whole set of points.

Keel development. The keel of the almond endocarp is the flat zone that lies on the side of the lateral view, surrounding the ventral suture . Depending on its size, the UPOV (2019) classifies it as weak, medium or strong (characteristic 38), as seen in Fig. 4. We follow the same concept, measuring its size numerically as the ratio of the area it spans relative to the full area of the endocarp.

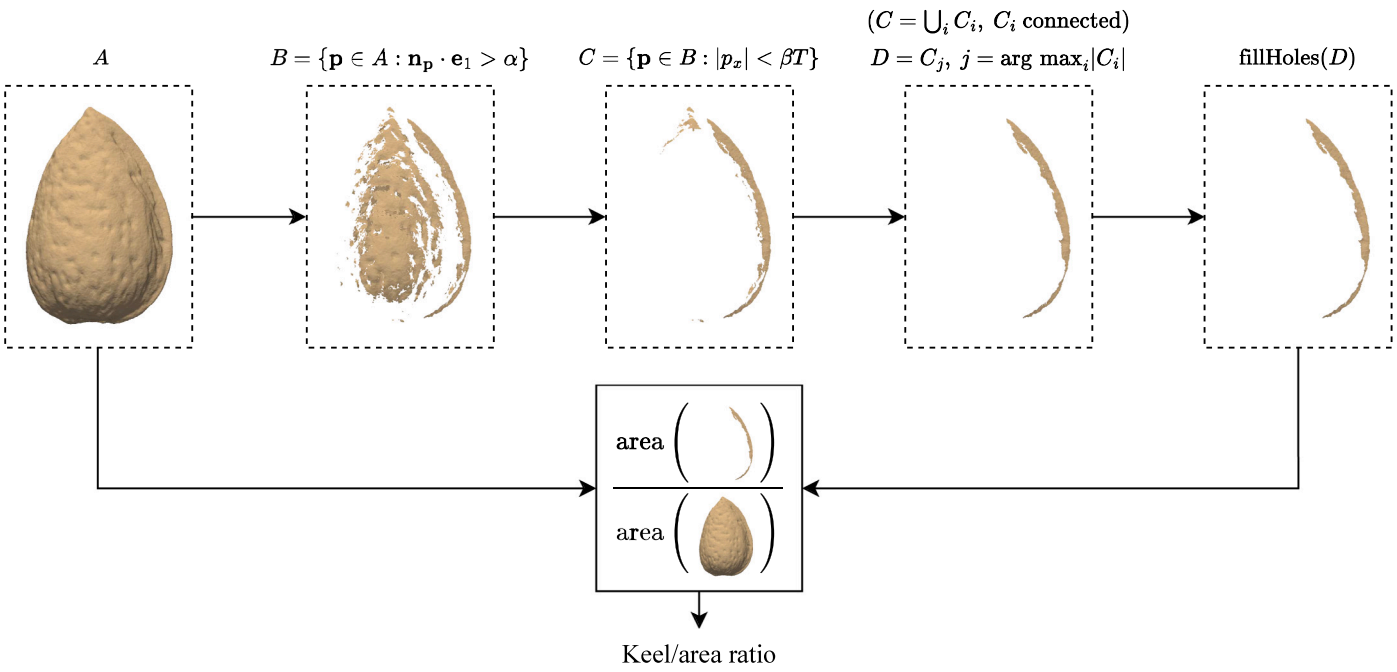

Fig. 10. Process for the description of the keel of the almond endocarp. Notation: $\mathbf{n_p}$ is the unitary normal vector of the surface at point $\mathbf{p}$; $\mathbf{e}_1$ is the vector $(1, 0, 0)$; p_x indicates the component x of point $\mathbf{p}$; α and β are thresholding parameters; T is the thickness of the endocarp.

Fig. 10 shows the procedure to detect the keel on the 3D mesh of an almond endocarp. We first search for points on its surface that are close in position to the ventral suture and in slope to the zy plane (i.e. points for which the cosinus of the angle their normal vector forms with $\mathbf{e}_1 = (1, 0, 0)$ is close to 1 and with an x coordinate close to 0). The set of selected points is an approximation of the keel, but can still encompass disconnected regions that are not necessarily part of it. Assuming that the majority of the keel has been correctly detected and that small, residual regions do not belong to it, we compute the connected components of the filtered mesh and only keep the biggest one. Finally, we fill the possible holes in that component that the first angular validation may have removed (Attene, 2010). We measure the area of the resulting submesh, divide it by the area of the endocarp, and return the value.

Markings on the surface. Almond endocarps can have pores and furrows on their surface. Although the UPOV does not specify any characteristic to describe them, the IBPGR (1985) establishes five different types of almond according to the markings of their endocarp: without pores, sparsely pored, intermediate, densely pored, and scribed (see Fig. 5). These categories, however, are subjective and difficult to quantify visually. They are also not mutually exclusive, as an almond endocarp can have both pores and furrows. As an alternative, we propose to describe the endocarp's markings by detecting and counting its pores and furrows over its surface area.

The algorithm for the detection of pores and furrows is illustrated in Fig. 11. Since the points we want to detect go inward into the endocarp, we begin by setting apart candidate points with a small minimum principal curvature (Mokhtarian et al., 2001). Not all of these points correspond to a single mark on the endocarp; some of them are false positives, while some detections are redundant and should belong to a unique pore or furrow. Knowing this, we discard points too close to the zy plane (which are likely to belong to the keel and ventral suture) and use the density-based clustering algorithm DBSCAN (Ester et al., 1996) to group nearby candidate points into single marks. We then remove clusters with too few members in order to reduce the number of false positives.

Visually, the way to distinguish between different types of marks is by their size: a pore is completely localized, whereas a furrow spans a curve over the surface of the shell. We translate this idea into our method by computing a Principal Component Analysis of the points contained in each cluster. We classify the clusters according to the proportion of variance explained by the first principal component: a small value corresponds to a pore, while a larger one means that the points sway significantly in a concrete direction, which is expected of a furrow.

Finally, given the number of clusters and their classification, we return the pore density as the number of pores over the total surface area, as well as the number of furrows.

Symmetry. Neither the UPOV nor the IBPGR establish any characteristic to describe the symmetry of the almond endocarp. Nonetheless, we can quantify it on the different views of the endocarp following the scheme in Fig. 12. A cut in two halves is done by the vertical line that passes through the origin and the apex on the front, back and lateral views, and by the zy plane on the top and bottom views. Then, the left side of the cut is reflected to the right side so that both halves overlap. The symmetry value of the respective view is given by the intersection over union area ratio of the halves.

4. Results and discussion

4.1. Translation from quantitative to qualitative descriptors

We compare the results of our methods with the currently available data by the IRFAP and the CITA on the scanned almond varieties. While our proposed descriptors yield numerical information of the features they describe, the descriptors provided by those institutions are purely qualitative, since they are based on the guidelines by the UPOV and the IBPGR. Thus, we first convert our quantitative values into the same qualitative UPOV and IBPGR descriptors by applying different thresholds. To minimize the influence of outliers, we assign descriptors by variety: for every feature, we compute its descriptor for each individual almond endocarp, and select the most common one inside a variety to describe it as a whole. We perform this translation for the descriptors of the contour shape, apex shape and keel development.

Contour shape. We use the states of expression defined by the IBPGR, which are richer than the UPOV's, as qualitative labels to

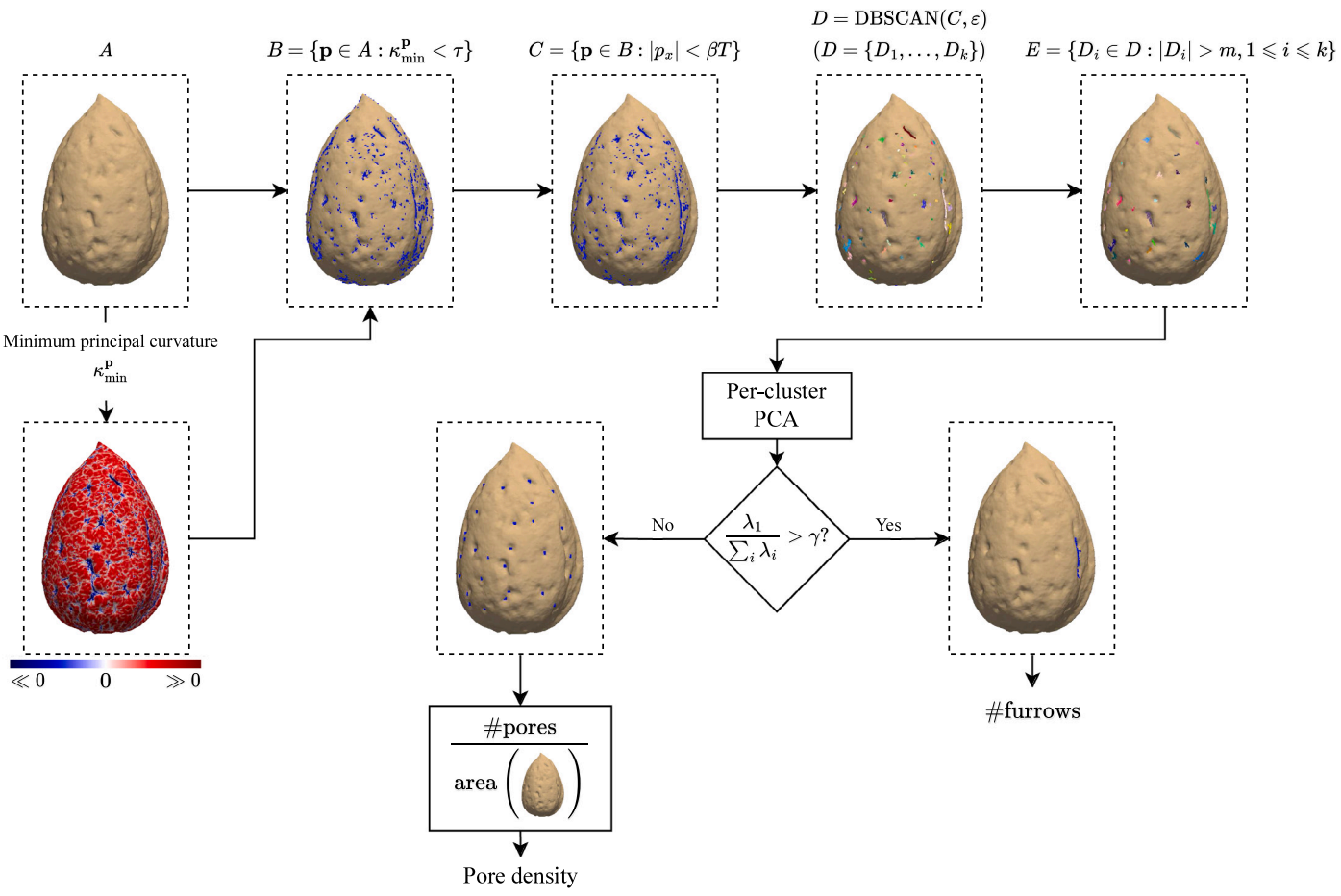

Fig. 11. Process for the description of the markings of the almond endocarp. This figure should be viewed in color, preferably on a computer screen. Notation: $\kappa^{\mathbf{p}}_{\min}$ is the minimum principal curvature at point $\mathbf{p}$; p_x indicates the component x of point $\mathbf{p}$; T is the thickness of the endocarp; τ, β, m and γ are thresholding parameters; ε is the neighbor-distance used by the DBSCAN algorithm; $\{\lambda_i\}$ are the eigenvalues of the PCA in decreasing order.

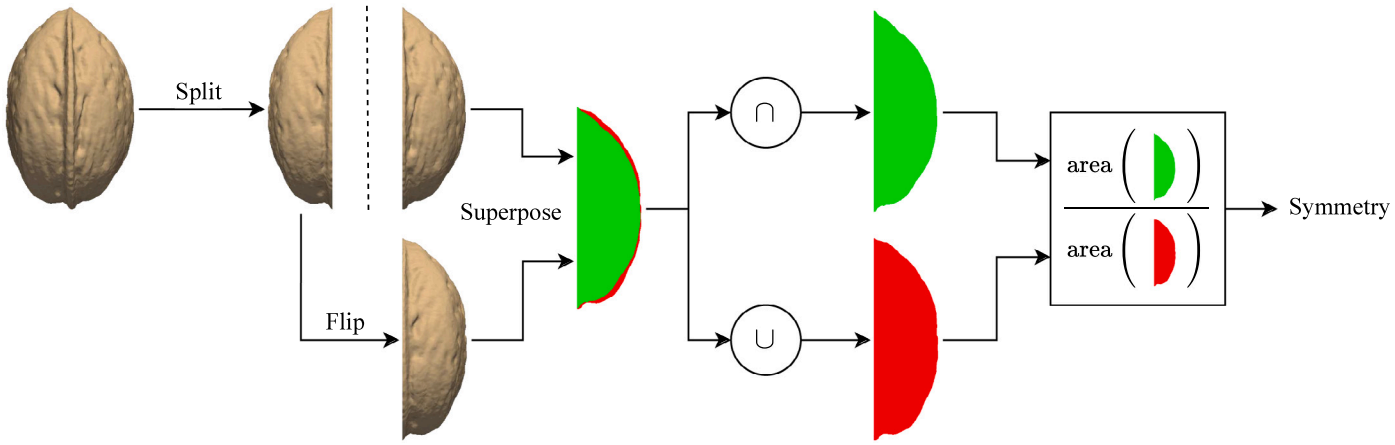

Fig. 12. Process for the description of the symmetry of the almond endocarp. The front view is used for illustration purposes; the process is done analogously for other views. This figure should be viewed in color. Notation: $\cap$ is the intersection of the superimposed halves of an almond view; $\cup$ is their union.

describe the contour shape of the endocarp. First, we discriminate by eccentricity. Those endocarps with a very high value (empirically, $e > 0.85$) should always be classified as extremely narrow. On the contrary, those with a very low value ($e < 0.6$) can be either round or ovate, so we use the ovacity to differentiate between the two. A value $\mathcal{O} < 0.02$ indicates that the center of mass is approximataly at the same height as the center of the circle containing the almond endocarp, so it can be considered round; the opposite means that it is ovate. The range of intermediate excentricity values is more complex, as oblong and cordate almond endocarps can have similar features. Generally, oblong endocarps have a higher excentricity and lower ovacity than cordate ones, but that is not always the case. We choose to classify endocarps with $0.6 \leqslant e \leqslant 0.75$ as oblong if $\mathcal{O} < 0.03$ and cordate otherwise, while we consider those with $0.75 < e \leqslant 0.85$ to be similar enough to an ellipse to always be classified as oblong.

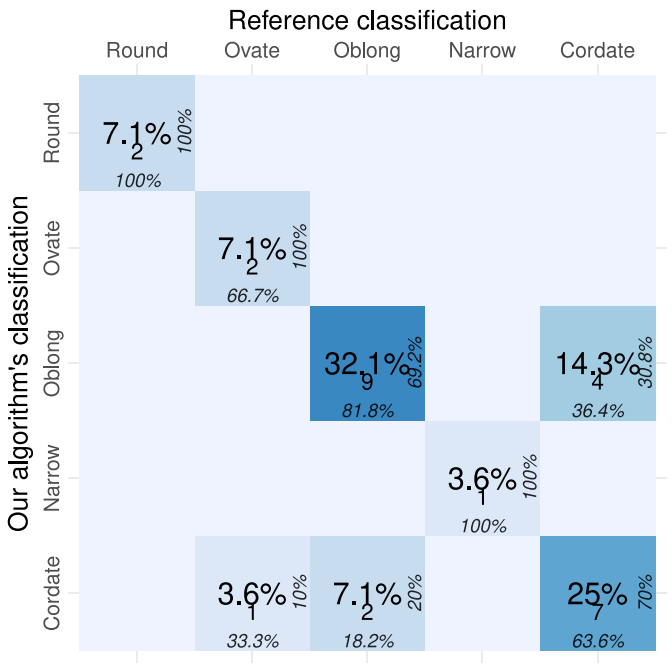

Fig. 13. Our description of the almond endocarp shapes (vertical axis) vs. data from the CITA obtained by visual evaluation (horizontal axis). The central percentage at each square represents the proportion of varieties in it over the total. The number below it counts the varieties in absolute terms. The right and bottom percentages represent their proportion over the row and column, respectively.

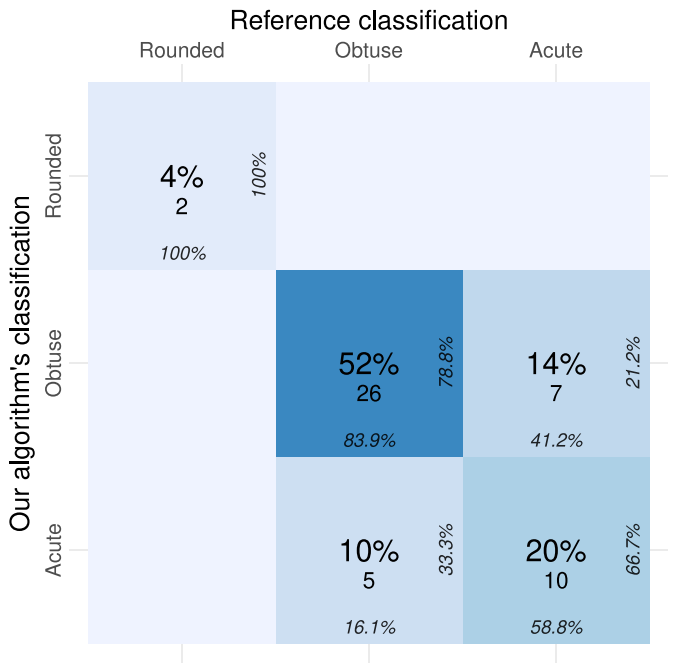

Fig. 14. Our description of the apex shapes (vertical axis) vs. data from the IRFAP and CITA obtained by visual evaluation (horizontal axis). The central percentage at each square represents the proportion of varieties in it over the total. The number below it counts the varieties in absolute terms. The right and bottom percentages represent their proportion over the row and column, respectively.

Apex shape. Apex shape is computed with the upper 7 % of points of the contour of the almond endocarp and transformed into the UPOV's classification. To categorize the results, we first look at the computed apex angle θ. Although the UPOV uses the words "acute" and "obtuse" to describe pointed apices, in truth these are not strictly mathematical terms and are used to mean only general closedness or openness. With that in consideration, we find that the condition $\theta < 102°$ works best to label "acute" apices. Larger angles can mean that the apex is either obtuse or rounded. In particular, we notice that endocarps with round apices tend to have very open angles in addition to a high measure of apex roundness. For this reason, to detect the latter we assert an apex roundness higher than 0.85 and an angle larger than 135°. Any other case is classified as obtuse.

Keel development. We measure keel development using the points of the endocarp mesh with an x coordinate value smaller (in absolute value) to the $\beta = 10\,\%$ of the endocarp thickness. A threshold of $\alpha = 0.9$ for the cosinus is used in the angular validation step to determine which points are candidates to be part of the keel. After computing the keel/area ratio, we consider a keel to be weak if the value is smaller than 0.018, strong if it is bigger than 0.08, and medium otherwise.

4.2. Comparison with reference institutional data

We assess the validity of the proposed descriptors by comparing our results with the characterizations by both the IRFAP and the CITA. All 50 varieties are used when comparing apex shape and keel development. However, since the IRFAP uses the UPOV's classification instead of the IBPGR's to describe the contour shape of the almond endocarp, we compare our results only with the CITA's data (28 varieties) for that characteristic.

Figs. 13 (contour shape), 14 (apex shape) and 15 (keel development) show the confusion matrices between our derived descriptors and those of the reference institutions. Each of them are respectively supported by visual results in Figs. 16, 17 and 18. At each square, the central percentage of these matrices corresponds to the percentage of

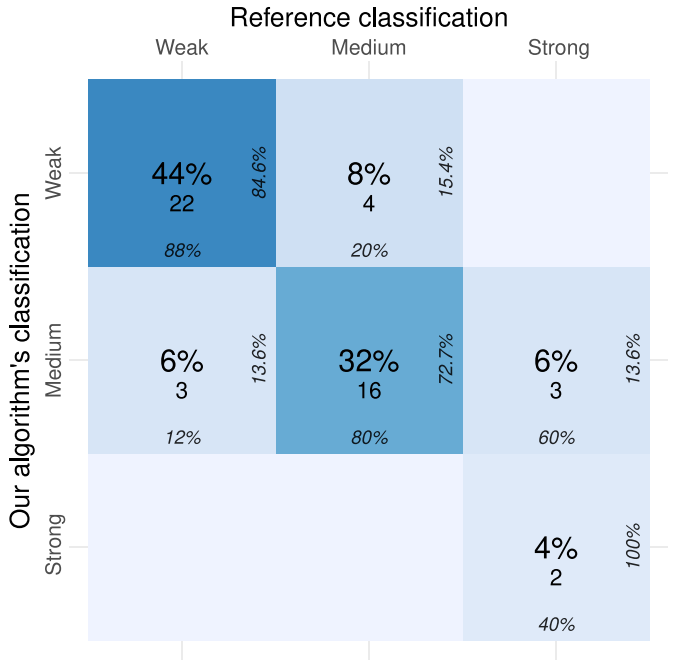

Fig. 15. Our description of the almond endocarp keels (vertical axis) vs. data from the IRFAP and CITA obtained by visual evaluation (horizontal axis). The central percentage at each square represents the proportion of varieties in it over the total. The number below it counts the varieties in absolute terms. The right and bottom percentages represent their proportion over the row and column, respectively.

varieties classified as the row name by our method and the column name by the reference data. The number below that percentage counts the number of varieties. For example, in Fig. 13, four varieties (14.3 % of the total) are classified as being oblong by our method and cordate

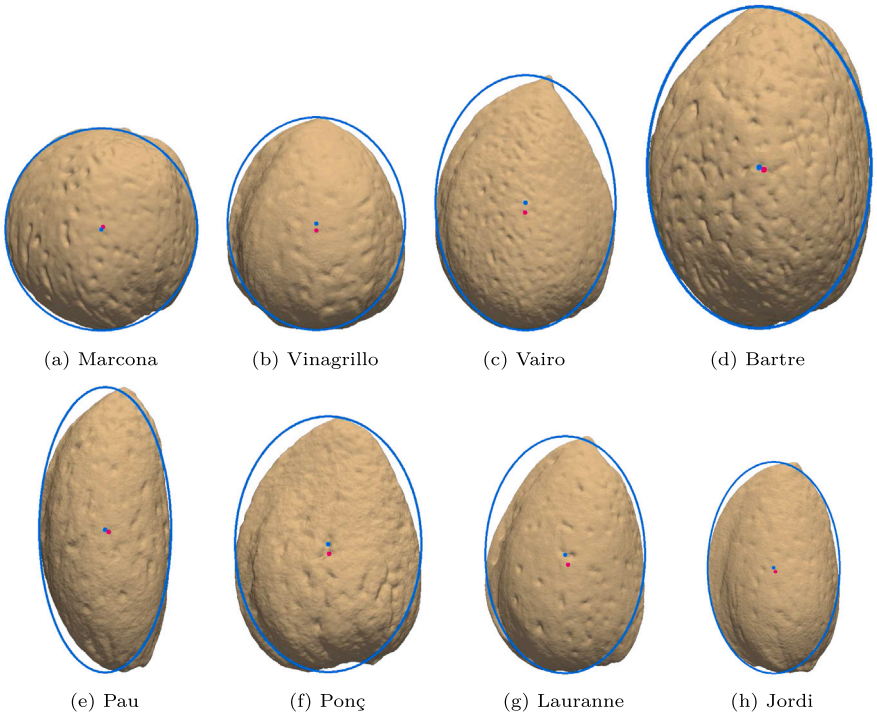

Fig. 16. Examples of almond endocarps of different contour shapes, as classified by our method. The eccentricity of each endocarp is the same as that of the blue ellipse with blue center. The center of mass is painted in red. (a): Round. (b): Ovate. (c): Cordate. (d): Oblong. (e): Extremely narrow. (f): Cordate, classified as ovate by the CITA. (g): Cordate, classified as oblong by the CITA. (h): Oblong, classified as cordate by the CITA.

by the CITA. The other two percentages correspond to the precision (right) and recall (down) of each pair of possible values.

The results on contour shape show that the proposed method coincides in most cases (21 out of 28, or 75.0 %, summing the diagonal entries in Fig. 13) with the reference descriptions. However, it mainly differs from the CITA when distinguishing between oblong and cordate almond endocarps. Taking a look at Figs. 16(g) and 16(h), we can find a possible explanation to that phenomenon in the visual ambiguity of some shapes, which can lead to inconsistent results during manual evaluation. Our method's classification is not affected by this kind of ambiguity, as it is based on objective quantitative measures: given two endocarps with the same excentricity and ovacity, they will always be labeled the same.

The descriptions of apex shapes, while they mostly coincide with the ones proposed by the IRFAP and the CITA (38 out of 50, a 76.0 % coincidence), yield slightly different results for pointed shapes. Particularly, Fig. 14 shows that there is low precision (66.7 %) and recall (58.8 %) when classifying acute apices. Rounded apices are all classified correctly without any confusion with other shapes. Visual results in Figs. 17(a) through 17(c) show examples of correctly classified apices of each kind, while Figs. 17(d) and 17(e) expose discrepancies in classification. Since we have already noted that the "acute" and "obtuse" categories defined by the UPOV do not correspond with their mathematical counterparts, it is possible that some differences in classification could be partly attributed to inconsistent manual categorization of edge cases caused by the lack of rigor in the definition of the labels. Using a fixed threshold for the apex angle, as we do, can reduce such inconsistencies.

Finally, in Fig. 15 it can be seen that the proposed method agrees with the CITA and IRFAP's description of the endocarp's keel in 40 out of 50 (80.0 %) almond varieties, although with a low recall in strong keels and with minor discrepancies between weak and medium ones. Examples of these are shown in Fig. 18.

4.3. Visual validation

The IRFAP does not provide data about the symmetry nor the markings of the endocarp of any of the varieties studied in this work. The CITA provides qualitative information on the symmetry of the bottom view of the almond endocarp, but it follows a different methodology than ours: what is measured is the deviation of the lower part of the keel from the symmetry axis instead of the proportion of area that falls on each side. Their classification of the markings of the endocarp also takes into account the size of the pores, which our algorithm does not. Furthermore, to the best of our knowledge, no other organization nor journal has published information on these features for the varieties we have used. For that reason, we have chosen to evaluate these feature descriptors only visually.

In Fig. 19 we observe the results of our pore detection algorithm on several almond endocarps. These results are obtained with a minimum principal curvature threshold of $\tau = -3.0\,\mathrm{mm}^{-1}$, a DBSCAN parameter of $\varepsilon = 0.25\,\mathrm{mm}$, and a variance proportion threshold of $\gamma = 0.95$ to distinguish between pores and furrows. From Figs. 19 to 19(d), we display almond endocarps with an increasing proportion of pores over their surface. Figs. 19(e) and 19(f) also present endocarps with a mixture of pores and furrows. Through a rough visual assessment, we see that our method produces a good estimation in terms of false detections (precision): detected pores tend to correspond to real pores of the endocarp. With respect to non-detected pores (recall), the method misses some of the detections, as seen in Figs. 19(c) and 19(d). However, as the almond variety becomes more pored, the number of detected pores also increases.

Finally, in Fig. 20 we can see the results on symmetry computation for two almond endocarps of different varieties. We paint the intersection of the mirrored left side and the right side of each view in green, and the rest of their union in red. It is clear that for symmetric endocarps, the areas almost coincide and as a consequence the intersection over union yields a value close to 1. Conversely, asymmetric endocarps attain a low value of the measure.

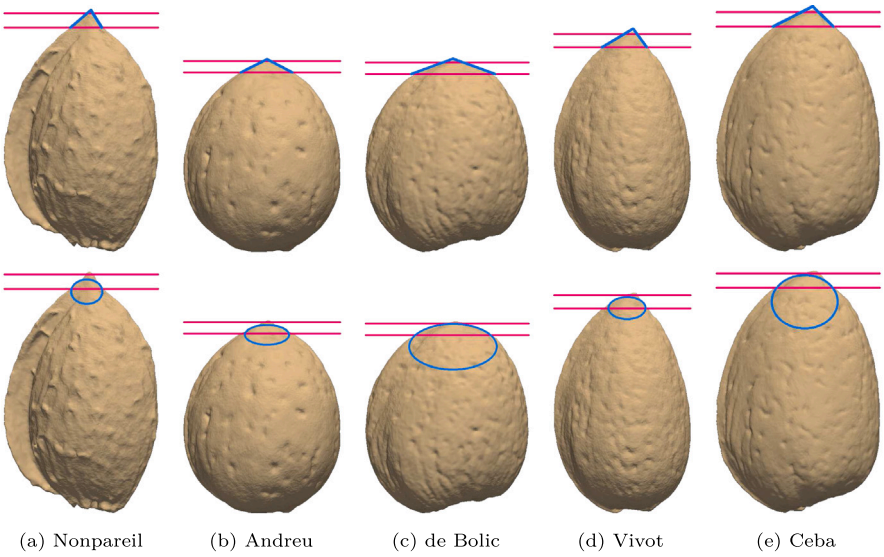

Fig. 17. Examples of different apex shapes, as classified by our method. The apex is delimited by the two red lines. The blue lines in the first row are used to compute the apex angle, while the blue ellipse in the second row is used to measure the apex roundness. (a): Acute. (b): Obtuse. (c): Rounded. (d): Acute, classified as obtuse by the CITA. (e): Obtuse, classified as acute by the IRFAP.

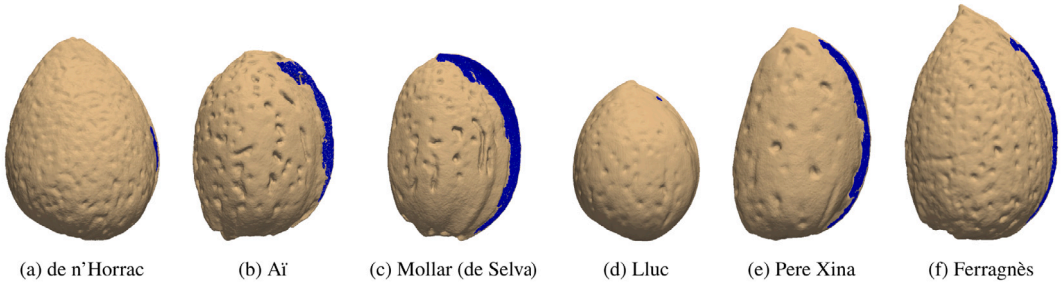

Fig. 18. Examples of different keel sizes, as classified by our method. This figure should be viewed in color. The blue area corresponds to the detected keel. (a): Weak. (b): Medium. (c): Strong. (d): Weak, classified as medium by the IRFAP. (e): Medium, classified as weak by the CITA. (f): Medium, classified as strong by the CITA.

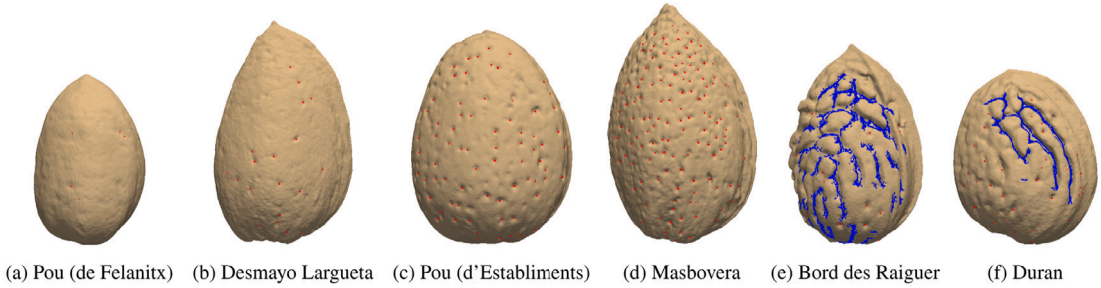

Fig. 19. Examples of different types of markings. This figure should be viewed in color, preferably on a computer screen. The detected pores are indicated with a red dot, while furrows are highlighted in blue. (a): Almost no pores. (b): Sparsely pored. (c): Intermediate pored. (d): Densely pored. (e): Scribed. (f): Pored + scribed.

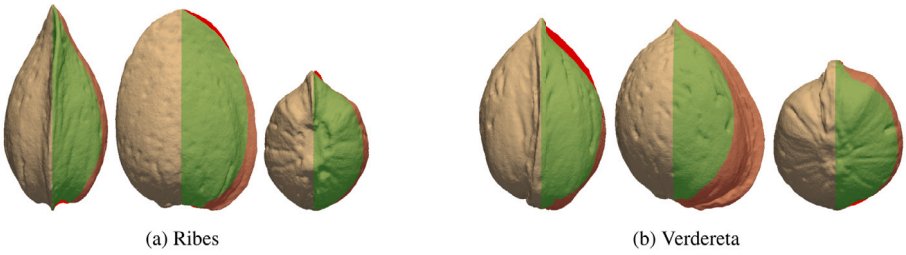

Fig. 20. Example of two different almond endocarps viewed from three different perspectives. This figure should be viewed in color. The green region is the intersection of the right side and the mirrored left side of the almond endocarp, while the red region is their union excluding the intersection. (a) has higher symmetry values than (b).

4.4. Limitations

The proposed method for the morphological description of the almond endocarp is a step forward in the automation of the process. The proposed feature extraction algorithms are fast, and have the advantage over classical approaches based on simple visual examination that they use objective measures to deal with ambiguity and favor consistency. However, these algorithms have the main limitation of requiring a correctly oriented 3D mesh of the almond endocarp as input. In this work, we have oriented the meshes manually. Although only three points need to be selected per mesh to do so, this can be a time consuming task if large amounts of data must be processed, and is an obstacle to automation. Automatically orienting the meshes by detecting the peduncle, apex and ventral suture with computer vision techniques could be a future line of work to resolve this bottleneck.

Another limitation is that, despite 3D scanning technology becoming more accessible, it is still more expensive and not yet as ubiquitous as 2D photography. Moreover, the quality of the meshes and the scanning speed can vary depending on the scanner and its software. For the proposed method to be useful in practice, the 3D scanner must be able to capture the surface of the almond endocarp with enough detail, and the captured meshes must be well-formed. For example, if an endocarp is partially broken (which is common in the case of varieties with soft endocarps) or the scan process produced errors, human intervention is required to identify these cases and discard them. Finally, scanning speed, albeit improving with the years, is still an issue for large-scale studies.

5. Conclusions

In this paper we have proposed a computer-vision-based methodology for the extraction and description of different features of the endocarp of the almond nut. We have collected almond endocarps from trees grown in the island of Mallorca—both from autochthonous and introduced varieties—and scanned them alongside samples from other imported varieties to form a dataset of 9510 3D endocarp meshes. Then, based on measures pertaining to the geometry of their surface, we have defined a set of continuous quantitative descriptors to characterize their contour shape, apex shape, keel development, markings, and symmetry—traits that have been traditionally computed by simple visual inspection. Validation with 2610 scanned endocarps from 50 different varieties has shown that the proposed method mostly agrees (75.0 % coincidence on contour shape, 76.0 % on apex shape, 80.0 % on keel development) with the qualitative descriptors registered by the Institut de Recerca i Formació Agroalimentària i Pesquera de les Illes Balears (IRFAP) and the Centro de Investigación y Tecnología Agroalimentaria de Aragón (CITA), both institutions that study germplasm collections. Discrepancies can mostly be attributed to the subjective nature of the traditional evaluation, which our method overcomes.

The proposed method could be further improved by automating the orientation of the 3D meshes to a common frame of reference, which is currently done manually. Detecting precisely the peduncle, apex and ventral suture based on their geometric characteristics could lead to a substantial speedup in the description process. Another possible line of future work is to use the proposed quantitative descriptors as a baseline for cultivar identification. Although the morphological characterization of the endocarp is not enough to identify a variety with certainty, complementing it with other types of data—such as tree vigor, texture of bark, density of foliage, leaf blade shape, kernel size and rugosity, and colorimetric information of the leaves, flower bud and kernel, among others—could offer the means to develop a more complete and reliable method for the identification of almond varieties.

CRediT authorship contribution statement

Marco Sánchez-Beeckman: Formal analysis, Methodology, Software, Validation, Visualization, Writing – original draft, Writing – review & editing. **Jaume Fornés Comas:** Data curation, Methodology, Resources, Writing – original draft, Writing – review & editing, Conceptualization. **Onofre Martorell:** Formal analysis, Methodology, Software, Writing – original draft, Writing – review & editing. **José M. Alonso Segura:** Supervision, Writing – review & editing. **Antoni Buades:** Supervision, Writing – review & editing.

Declaration of competing interest

The authors declare that they have no known competing financial interests or personal relationships that could have appeared to influence the work reported in this paper.

Data availability

Data will be made available on request.

Acknowledgments

We want to give our thanks to Antoni Moragues, Mateu Ferrer, Bartomeu Vallespir and Cristòfol Rotger for their help on the process of scanning, and to Josep A. Rosselló (Universitat de València) for his valuable counsel. We also want to show our appreciation to Federico Dicenta (CBAS-CSIC), Agustí Romero (IRTA), Manuel Puebla (CICYTEX) and Thomas M. Gradziel (UC Davis) for sending us samples of nuts of different almond varieties, as well as to Productors Mallorquins de Fruits Secs S.A.T. for lending us their facilities to store the materials used for the experimentation. We extend our gratitude to the farmers and plantation owners for their selfless help and for allowing us to collect their almonds. Finally, we want to acknowledge the Ajuntament de Santa Margalida, Aart Jan Hemmink and Fundación MarViva for their support.

This publication is funded by MCIN/AEI/10.13039/501100011033 and by "ERDF A way of making Europe", European Union, under grant PID2021-1257110B-I00.

Marco Sánchez-Beeckman is also supported by the Conselleria de Fons Europeus, Universitat i Cultura del Govern de les Illes Balears through grant FPU2023-011-C.

References

Anders, A., Choszcz, D., Markowski, P., Lipiński, A.J., Kaliniewicz, Z., Ślesicka, E., 2019. Numerical modeling of the shape of agricultural products on the example of cucumber fruits. Sustainability 11 (10), 2798. http://dx.doi.org/10.3390/su11102798.

Antonucci, F., Costa, C., Pallottino, F., Paglia, G., Rimatori, V., de Giorgio, D., Menesatti, P., 2012. Quantitative method for shape description of almond cultivars (*Prunus amygdalus* Batsch). Food Bioprocess Technol. 5 (2), 768–785. http://dx.doi.org/10.1007/s11947-010-0389-2.

Ardjmand, A., Piri, S., Imani, A., Piri, S., 2014. Evaluation of morphological and pomological diversity of 62 almond cultivars and superior genotypes in Iran. J. Nuts.

Attene, M., 2010. A lightweight approach to repairing digitized polygon meshes. Vis. Comput. 26 (11), 1393–1406. http://dx.doi.org/10.1007/s00371-010-0416-3.

Barreca, D., Nabavi, S.M., Sureda, A., Rasekhian, M., Raciti, R., Silva, A.S., Annunziata, G., Arnone, A., Tenore, G.C., Süntar, İ., et al., 2020. Almonds (Prunus dulcis Mill. DA Webb): A source of nutrients and health-promoting compounds. Nutrients 12 (3), 672.

Benarous, A.O.F., 2020. Almond Variety Detection Using Deep Learning (Ph.D. thesis). Instituto Politécnico de Bragança, URL http://hdl.handle.net/10198/23220.

Blazakis, K.N., Kosma, M., Kostelenos, G., Baldoni, L., Bufacchi, M., Kalaitzis, P., 2017. Description of olive morphological parameters by using open access software. Plant Methods 13 (1), 1–15. http://dx.doi.org/10.1186/s13007-017-0261-8.

Chalak, L., Chehade, A., Kadri, A., 2007. Morphological characterization of cultivated almonds in Lebanon. Fruits 62 (3), 177–186. http://dx.doi.org/10.1051/fruits:2007013.

Colic, S., Rakonjac, V., Zec, G., Nikolic, D., Aksic, M.F., 2012. Morphological and biochemical evaluation of selected almond [*Prunus dulcis* (Mill.) DA Webb] genotypes in northern Serbia. Turk. J. Agric. For. 36 (4), 429–438. http://dx.doi.org/10.3906/tar-1103-50.

Corkidi, G., Balderas-Ruíz, K., Taboada, B., Serrano-Carreón, L., Galindo, E., 2006. Assessing mango anthracnose using a new three-dimensional image-analysis technique to quantify lesions on fruit. Plant Pathol. 55 (2), 250–257. http://dx.doi.org/10.1111/j.1365-3059.2005.01321.x.

Costa, C., Antonucci, F., Pallottino, F., Aguzzi, J., Sun, D.W., Menesatti, P., 2011. Shape analysis of agricultural products: a review of recent research advances and potential application to computer vision. Food Bioprocess technol. 4 (5), 673–692. http://dx.doi.org/10.1007/s11947-011-0556-0.

de Giorgio, D., Leo, L., Zacheo, G., Lamascese, N., 2007. Evaluation of 52 almond (*Prunus amygdalus* Batsch) cultivars from the Apulia region in Southern Italy. J. Hortic. Sci. Biotechnol. 82 (4), 541–546. http://dx.doi.org/10.1080/14620316.2007.11512271.

Demir, B., Sayinci, B., Çetin, N., Yaman, M., Çömlek, R., 2019. Shape discrimination of almond cultivars by Elliptic Fourier descriptors. Erwerbs-Obstbau 61 (3), 245–256. http://dx.doi.org/10.1007/s10341-019-00423-7.

Ding, W., Nesumi, H., Takano, Y., Ukai, Y., 2000. Quantitative evaluation of the three-dimensional fruit shape and size of *Citrus* species based on spherical harmonic descriptors. Euphytica 114 (2), 103–115. http://dx.doi.org/10.1023/A:1003963214304.

El Hamzaoui, A., Oukabli, A., Moumni, M., 2014. Morphological and molecular diversity and genetic structure of Moroccan cultivated almond (*Prunus dulcis* Mill.) beside some foreign varieties. Plant Genet. Resour. 12 (3), 308–316. http://dx.doi.org/10.1017/S1479262114000094.

Ercisli, S., Sayinci, B., Kara, M., Yildiz, C., Ozturk, I., 2012. Determination of size and shape features of walnut (*Juglans regia L.*) cultivars using image processing. Sci. Hort. 133, 47–55. http://dx.doi.org/10.1016/j.scienta.2011.10.014.

Ester, M., Kriegel, H.P., Sander, J., Xu, X., et al., 1996. A density-based algorithm for discovering clusters in large spatial databases with noise. In: Proceedings of the Second International Conference on Knowledge Discovery and Data Mining. pp. 226–231. http://dx.doi.org/10.5555/3001460.3001507.

Esterlich, P., 1907. El almendro y su cultivo en el mediodía de España e Islas Baleares. Hijos de J. Cuesta, Madrid.

Fischler, M.A., Bolles, R.C., 1981. Random sample consensus: a paradigm for model fitting with applications to image analysis and automated cartography. Commun. ACM 24 (6), 381–395. http://dx.doi.org/10.1145/358669.358692.

Food and Agriculture Organization of the United Nations, 2023. FAOSTAT database. https://www.fao.org/faostat/en/#data/QCL. (Accessed 12 June 2023).

Fornés Comas, J., Socias i Company, R., Alonso Segura, J.M., 2019. Shell hardness in almond: Cracking load and kernel percentage. Sci. Hort. 245, 7–11. http://dx.doi.org/10.1016/j.scienta.2018.09.075.

Gouta, H., Mars, M., Gouiaa, M., Ghrab, M., Zarrouk, M., Mliki, A., 2009. Genetic diversity of almond (*Prunus amygdalus* Batsch) in Tunisia: A morphological traits analysis. In: V International Symposium on Pistachios and Almonds. pp. 351–358. http://dx.doi.org/10.17660/ActaHortic.2011.912.51.

Gradziel, T.M., 2010. Origin and dissemination of almond. In: Horticultural Reviews. John Wiley & Sons, Ltd, pp. 23–81. http://dx.doi.org/10.1002/9780470872376.ch2.

Grasselly, C., Crossa-Raynaud, P., 1980. L'Amandier. G. P. Maisonneuve et Larose.

Halac, D., Sokic, E., Turajlic, E., 2017. Almonds classification using supervised learning methods. In: 2017 XXVI International Conference on Information, Communication and Automation Technologies. ICAT, IEEE, pp. 1–6. http://dx.doi.org/10.1109/ICAT.2017.8171603.

Halíř, R., Flusser, J., 1998. Numerically stable direct least squares fitting of ellipses. In: 6th International Conference in Central Europe on Computer Graphics and Visualization, Vol. 98. pp. 125–132.

He, J.Q., Harrison, R.J., Li, B., 2017. A novel 3D imaging system for strawberry phenotyping. Plant Methods 13 (1), 1–8. http://dx.doi.org/10.1186/s13007-017-0243-x.

IBPGR, 1985. In: Gülcan, R. (Ed.), Descriptor list for almond (*Prunus amygdalus*) (Revised). International Board for Plant Genetic Resources, URL https://hdl.handle.net/10568/72793.

International Nut & Dried Fruit, 2023. Almonds global statistical review. https://inc.nutfruit.org/almonds-global-statistical-review-2/. (Accessed 15 June 2023).

Iwata, H., Ukai, Y., 2002. SHAPE: a computer program package for quantitative evaluation of biological shapes based on elliptic Fourier descriptors. J. Heredity 93 (5), 384–385. http://dx.doi.org/10.1093/jhered/93.5.384.

Kusumi, A., Nishiyama, S., Tao, R., 2023. Three-dimensional fruit growth analysis clarifies developmental mechanisms underlying complex shape diversity in persimmon fruit. J. Exp. Botany http://dx.doi.org/10.1093/jxb/erad472.

Kusumi, A., Osako, Y., Nakano, R., Nishiyama, S., Tao, R., 2021. Phenotypic evaluation of shape diversity in persimmon fruit using two-and three-dimensional imaging. In: VII International Symposium on Persimmon. pp. 263–268. http://dx.doi.org/10.17660/ActaHortic.2022.1338.38.

Li, B., Cockerton, H.M., Johnson, A.W., Karlström, A., Stavridou, E., Deakin, G., Harrison, R.J., 2020. Defining strawberry shape uniformity using 3D imaging and genetic mapping. Hortic. Res. 7, http://dx.doi.org/10.1038/s41438-020-0337-x.

Lovicu, G., Pala, M., De Pau, L., Satta, D., Pintore, R., Sedda, M., 2001. Fruit quality characteristics and productive behaviour in sardinian almond germplasm. In: III International Symposium on Pistachios and Almonds. pp. 493–497. http://dx.doi.org/10.17660/ActaHortic.2002.591.74.

Manolikaki, I., Sergentani, C., Tul, S., Koubouris, G., 2022. Introducing three-dimensional scanning for phenotyping of olive fruits based on an extensive germplasm survey. Plants 11 (11), 1501. http://dx.doi.org/10.3390/plants11111501.

Miho, H., Pagnotta, G., Hitaj, D., De Gaspari, F., Mancini, L.V., Koubouris, G., Godino, G., Hakan, M., Muñoz Diez, C., 2024. OliVaR: Improving olive variety recognition using deep neural networks. Comput. Electron. Agric. 216, 108530. http://dx.doi.org/10.1016/j.compag.2023.108530.

Mohamadi, A., Ghazavi, M., Hosseinzadeh, B., 2010. Determining regression models of almond and its kernel mass based on geometric properties (Shahrud 12 and mama'e varieties). J. Am. Sci. 6, 59–64.

Mokhtarian, F., Khalili, N., Yuen, P., 2001. Curvature computation on free-form 3-D meshes at multiple scales. Comput. Vis. Image Underst. 83 (2), 118–139. http://dx.doi.org/10.1006/cviu.2001.0919.

Moralejo, E., Gomila, M., Montesinos, M., Borràs, D., Pascual, A., Nieto, A., Adrover, F., Gost, P.A., Seguí, G., Busquets, A., et al., 2020. Phylogenetic inference enables reconstruction of a long-overlooked outbreak of almond leaf scorch disease (*Xylella fastidiosa*) in Europe. Commun. Biol. 3 (1), 1–13. http://dx.doi.org/10.1038/s42003-020-01284-7.

Morey, A., Fornés Comas, J., 2021. El cultivo tradicional del almendro en el Mediterráneo: Baleares en el contexto español (ca. 1770-2017). Hist. Agrar. 84, 103–140. http://dx.doi.org/10.26882/histagrar.084e01m.

Oliveira, I., Meyer, A., Afonso, S., Ribeiro, C., Gonçalves, B., 2018. Morphological, mechanical and antioxidant properties of Portuguese almond cultivars. J. Food Sci. Technol. 55 (2), 467–478. http://dx.doi.org/10.1007/s13197-017-2955-3.

Ponce, J.M., Aquino, A., Millán, B., Andújar, J.M., 2018. Olive-fruit mass and size estimation using image analysis and feature modeling. Sensors 18 (9), 2930. http://dx.doi.org/10.3390/s18092930.

Rodríguez, G.R., Moyseenko, J.B., Robbins, M.D., Morejón, N.H., Francis, D.M., van der Knaap, E., 2010. Tomato Analyzer: a useful software application to collect accurate and detailed morphological and colorimetric data from two-dimensional objects. JoVE (J. Vis. Exp.) 37, e1856. http://dx.doi.org/10.3791/1856.

Sacarès i Mulet, J., 1992. D'ametlers i conradors. Notes disperses. In: Miscelùlània d'homenatge a Sebastià Cardell i Tomàs. Edicions de pinte en ample, Llucmajor.

Sakai, N., Yonekawa, S., 1992. Three-dimensional image analysis of the shape of soybean seed. J. Food Eng. 15 (3), 221–234. http://dx.doi.org/10.1016/0260-8774(92)90052-8.

Sakar, E.H., El Yamani, M., Rharrabti, Y., 2019. Geometrical traits in almond fruit as affected by genotypic and environmental variations in Northern Morocco. Erwerbs-Obstbau 61 (2), 103–112. http://dx.doi.org/10.1007/s10341-018-0401-y.

Sarigu, M., Grillo, O., Bianco, M.L., Ucchesu, M., d'Hallewin, G., Loi, M.C., Venora, G., Bacchetta, G., 2017. Phenotypic identification of plum varieties (*Prunus domestica L.*) by endocarps morpho-colorimetric and textural descriptors. Comput. Electron. Agric. 136, 25–30. http://dx.doi.org/10.1016/j.compag.2017.02.009.

Sepahvand, E., Khadivi-Khub, A., Momenpour, A., Fallahi, E., 2015. Evaluation of an almond collection using morphological variables to choose superior trees. Fruits 70 (1), 53–59. http://dx.doi.org/10.1051/fruits/2014044.

Socias i Company, R., Alonso, J.M., Kodad, O., Gradziel, T.M., 2012. Almond. In: Fruit Breeding. Springer, pp. 697–728. http://dx.doi.org/10.1007/978-1-4419-0763-9_18.

Socias i Company, R., Felipe, A., 1992. Almond: A diverse germplasm. HortScience 27 (7), 718–863. http://dx.doi.org/10.21273/HORTSCI.27.7.718.

Sullivan, B., Kaszynski, A., 2019. PyVista: 3D plotting and mesh analysis through a streamlined interface for the Visualization Toolkit (VTK). J. Open Source Softw. 4 (37), 1450. http://dx.doi.org/10.21105/joss.01450.

UPOV, 2002. TG/1/3 - General Introduction to the Examination of Distinctness, Uniformity and Stability and the Development of Harmonized Descriptions of New Varieties of Plants. Technical Report, UPOV, p. 26.

UPOV, 2019. TG/56/4 Corr. Rev. Almond - *Prunus dulcis* (Mill.) D.A. Webb. Guidelines for the Conduct of Tests for Distinctness, Uniformity and Stability. Technical Report, UPOV, p. 31.

Vázquez-Arellano, M., Griepentrog, H.W., Reiser, D., Paraforos, D.S., 2016. 3-D imaging systems for agricultural applications—a review. Sensors 16 (5), 618. http://dx.doi.org/10.3390/s16050618.

Whan, A.P., Smith, A.B., Cavanagh, C.R., Ral, J.-P.F., Shaw, L.M., Howitt, C.A., Bischof, L., 2014. GrainScan: a low cost, fast method for grain size and colour measurements. Plant Methods 10 (1), 1–10. http://dx.doi.org/10.1186/1746-4811-10-23.

Zhang, C., Chen, T., 2001. Efficient feature extraction for 2D/3D objects in mesh representation. In: Proceedings 2001 International Conference on Image Processing (Cat. No. 01CH37205), Vol. 3. IEEE, pp. 935–938. http://dx.doi.org/10.1109/ICIP.2001.958278.

Zhang, Y., Wu, L., 2012. Classification of fruits using computer vision and a multiclass support vector machine. Sensors 12 (9), 12489–12505. http://dx.doi.org/10.3390/s120912489.